Refractory Plasmonic Material based Floating Solar Still for Simultaneous Desalination and Electricity Generation

Matthew J. Margeson, Mark Atwood, Jaser Lara de Larrea, Joseph Weatherby, Heather Daurie, Katlyn Near, Graham A. Gagnon, and Mita Dasog*

M. J. Margeson,[1] M. Atwood,[1] K. Near,[1] Prof. Dr. M. Dasog[1]
[1]Department of Chemistry, Dalhousie University, 6274 Coburg Road, Halifax, B3H 4R2, Canada
E-mail: mita.dasog@dal.ca

J. Lara de Larrea,[2] H. Daurie,[2] Prof. Dr. G. A. Gagnon[2]
[2]Centre for Water Resources Studies, Department of Civil and Resource Engineering, Dalhousie University, 1360 Barrington Street, Halifax, NS, B3H 4R2, Canada

Keywords: Desalination, solar evaporation, plasmonics, carbides, thermoelectricity

ABSTRACT

Established desalination technologies such as thermal distillation and reverse osmosis require advanced infrastructure and costly installation limiting their widespread implementation. Floating interfacial solar evaporation devices are considered a land-saving, environmentally friendly, and low infrastructure approach for freshwater production. Addressing issues related to maximum heat localization, prevention of salt accumulation and operating under stressful environmental conditions are some of the major challenges with floating solar desalination. This project presents an experimental demonstration of a plasmonic TiC nanoparticle-based floating solar still that can operate continuously under sunlight to produce clean water while floating on saline water sources. All materials, such as the PVC plastic condensation dome, EVA foam support, cotton wicks, and polyester filter fabric were chosen carefully to maximize the freshwater output of the solar still. The outdoor experiments were conducted in Halifax, Canada, where modest solar insolation of around 6 kW m^{-2} day^{-1} led to daily water yields up to 3.67 L m^{-2}. The water can be produced at costs as low as \$0.0086 L^{-1}, and the solar still can be easily modified to generate thermoelectricity. This could allow for small onboard devices to test water quality without the need for an external electricity source. The results of this study will contribute to further development of floating solar desalination to provide potable water for water-stressed communities.

1. Introduction

One of the largest ongoing humanitarian concerns is the growing demand for sustainable and economical clean water generation technology.[1,2] Desalination has emerged as one of the leading solutions to generate potable water.[3] Thermal distillation and reverse osmosis (RO) membrane separation are well developed techniques to purify saltwater, though generally require centralized and infrastructurally demanding treatment plants.[4–8] These are tied to high energy consumption and major economic investments which restricts broad use, particularly in developing countries or remote locations.[9,10] This has caused a surge in alternative water purification technologies, and desalination using abundantly available solar energy has become an attractive method to improve water security in these regions.[11] Most notable are floating solar evaporation units as they can be deployed directly on a water source and require no land use.[12,13] Floating solar evaporation often uses strong light absorbers, known as photothermal materials to convert sunlight into heat used for evaporation. Over the years, many different platforms have been tested, with the most efficient using interfacial evaporation as opposed to bottom heating or bulk heating where thermal losses are much higher (Figure 1).[14]

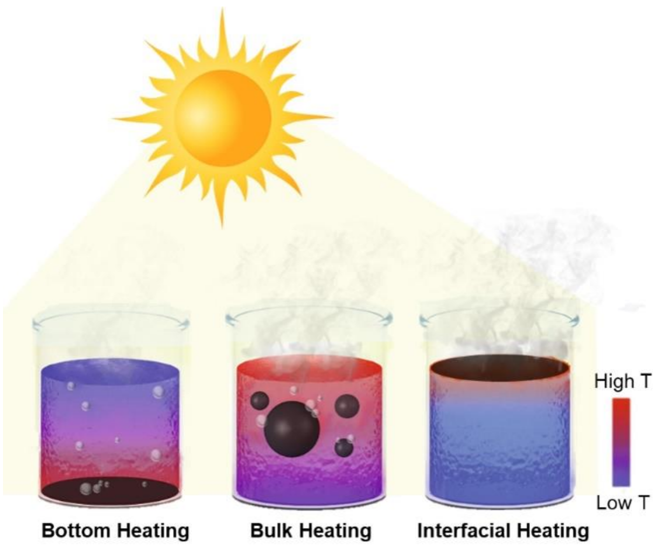

Figure 1: Schematic of different solar vapor generation layouts using photothermal materials.

Reaching high efficiencies with floating desalination units requires high absorption of the incoming solar energy, effective thermal management to prevent heat loss, and avoiding salt buildup and contamination of the evaporation surface.[15,16] Heat localization is achieved by insulating the evaporation interface from the bulk water below to avoid heat loss and instead transfers that energy to the small volume of water on the surface.[17] Wicking structures that provide sufficient flow of water across the evaporation surface via capillary action have been shown to avoid buildup of salt and other contaminants that might affect long term desalination efficiency.[18] Increases in the amount of sunlight absorbed for conversion to heat is a material consideration, and many light-to-heat conversion (or photothermal) materials have been developed. These range from carbonaceous materials[19–21] to thermally conductive polymers,[22,23] semiconductors,[24,25] and plasmonic nanomaterials.[26,27] Many of these effectively absorb ≥90% of the solar spectrum, with corresponding solar to vapor generation efficiencies greater than 85%, and have been summarized in recent reviews.[28,29] Plasmonic nanomaterials are particularly suitable for photothermal application as they can produce intense localized heat from their interaction with incident light.[30] Recently, refractory plasmonic nitrides and carbides have garnered significant attention for desalination application given their superior photothermal properties, low cost, and material stability.[31–34]

Most floating solar desalination research has been done only in controlled lab environments, with real-world studies remaining scarce.[35–39] To avoid stagnation of the field and to prove the potential for floating desalination, it is important to test promising materials in a real-world setting. This brings to the forefront new challenges associated with material preparation, overall efficiency, and deployment.[40,41] Some of the more elaborate material compositions and designs tested in lab will not be feasible to scale up economically.[42–46] Additionally, having a vapor collection system, convective cooling from ocean currents and waves, and increased humidity within the collection system can all take a toll on the efficiency. These factors are all in addition to retaining salt rejection capabilities. This has caused drastic decreases for previously reported floating solar stills from ~90% to below 20% in most cases.[47-50]

Nevertheless, several groups have undertaken these challenges. Gan *et al.* reported a floating solar still using carbon coated paper on top of a polystyrene support that resulted in a freshwater yield of 0.8 L m^{-2} day^{-1}.[51] Unfortunately, the accumulation of salt on the surface is thought to have decreased the efficiency over time. Since then, Chen *et al*. have designed a desalination still capable of salt-rejection during continuous use.[52] This device employed a large wicking area (~20%), and a freshwater production rate of 2.5 L m^{-2} day^{-1} was achieved. The solar still also benefitted from a low material cost of \$3 m^{-2}, putting it over an order of magnitude lower than conventional land solar stills. A root inspired solar still from Xie et al. demonstrated that a 1-dimensional wick system could decrease the required wicking area to only 2% while maintaining salt rejection.[53] This afforded a freshwater generation rate of 1.5 L m^{-2} day^{-1}. A floating solar still by Aye et al. used a vacuum pump to increase their freshwater yield to 4.3 L m^{-2} day^{-1}, unfortunately this removed the passive nature of the solar still as it required an electrical plug to operate, increasing complexity and cost.[54] A final benefit to a floating desalination system is the potential to simultaneously generate thermoelectric power. Taking advantage of the temperature gradient between the evaporation surface and the colder ocean water below using the Seebeck effect, a current can be generated by placing Peltier modules across the platform. While this has been explored in a lab setting and suggested for incorporating into a floating solar still, there has yet to be experimental results to date for a scaled-up process.[55–57]

Herein, we develop a titanium carbide (TiC) nanoparticle (NP) based floating solar still engineered to address the previously discussed technical obstacles. One of the key precursors for the synthesis of TiC NPs, amorphous carbon, is made through the pyrolysis of waste tire rubber making this a useful synthetic method from a recyclability standpoint. The solar still is capable of efficiently generating freshwater long term without suffering from salt buildup or large thermal loss. The design maintains operational stability with wind, waves, and currents. The obtained freshwater was tested for microbe activity and a variety of potential contaminants found in the source water. Additional modification of the solar still allows for the practical generation of thermoelectric power, which was shown to run small devices and could be incorporated as on-board water quality sensors in the future. The research is expected to highlight the potential for floating desalination as an alternative to land solar stills for solar desalination.

2. Results and Discussion

2.1 Material Synthesis and Evaporation Interface Preparation

Char derived from waste tire rubber and plasmonic TiC nanoparticles (NPs) were prepared using a modified previously reported method.[58,59] The schematic of the material synthesis and interface fabrication is shown in Figure 2. In short, tires were ground into a fine rubber crumb before undergoing pyrolysis at 500 °C for 1 h under inert atmosphere to form amorphous carbon (Figure S1). Afterwards, the reaction mix was treated with concentrated HNO_3 (aq), followed by thorough washing in deionized water to yield porous carbon particles. This appeared to be a mixture of larger porous carbon particles 14 ± 4 μm in size with a couple larger particles reaching up to 50 μm (Figure S2A) and areas of smaller carbon particles >100 nm (Figure S2B). These smaller particles are likely carbon black which is used as an additive in tire manufacturing. It is important to note that tires are not a desired item to end up at landfills, as they can leach chemicals into the ground and nearby water sources. It is critical to find ways to properly recycle them at the end of their life. The pyrolysis of waste tire rubber is an attractive way to lock the carbon in its elemental form and to safely remove other fillers such as sulfur, silica, etc.[60] Using the amorphous carbon to create a value-added material makes the proposed TiC NPs very interesting to recycle waste tire rubber.

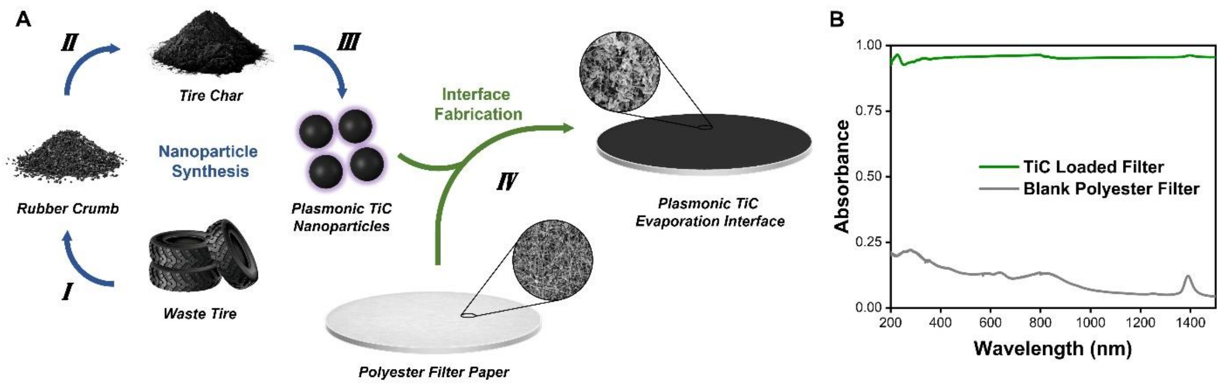

Figure 2: (A) Schematic of TiC NP synthesis and evaporation interface fabrication. Steps shown: (I) Tire shredding. (II) Pyrolysis of rubber crumb at 500 ^{o}C under inert atmosphere. (III) TiC production by magnesiothermic reduction reaction of TiO_2 in the presence of Mg powder and tire char at 900 ^{o}C in Ar atmosphere. (IV) Vacuum loading of TiC NPs onto porous filter paper. Insets show SEM images before and after loading of TiC. (B) Absorbance spectra of TiC interface (green) and blank polyester interface (grey).

The resulting char was ground with TiO_2 and Mg powder until homogeneous. The mixture was then reacted under Ar at 950 °C for 2 h. After cooling, the MgO side product and any unreacted Mg was removed by sonicating the reaction mixture in 6.0 M HCl. The powder X-ray diffraction pattern of the product showed only peaks corresponding to the rocksalt structured TiC (Figure S3). The transmission electron microscopy showed the NPs to have an average diameter of 12 ± 5 nm (Figure S4). Previous calculations have shown the localized surface plasmon resonance (LSPR) maximum of TiC NPs with 10 - 15 nm diameter to be below 150 nm.[32] The absorbance spectrum of TiC NPs suspended in water (Figure S5) corroborated with the calculations and the distinctive LSPR maximum is beyond the instrument detection range. After thoroughly drying, the TiC NPs were vacuum loaded onto a large and porous polyester filter using a vacuum box constructed in house (Figure S6). SEM images were taken before and after TiC NPs were loaded onto the interface, which can be seen in the insets of Figure 2A and shown fully in Figure S7. Polyester filter paper was chosen as a low-cost material, and for its widespread availability and porosity. After loading the NPs onto the polyester filter paper, the absorbance of the plasmonic interface broadened significantly to absorb over 95% of the light between 200 – 1200 nm (Figure 2B). This is due to the plasmonic coupling between particles within close proximity as shown in calculations performed previously on carbide NPs.[32]

2.2 Desalination Experiments in Rooftop Pool and Ocean

The TiC interface was then placed within the floating solar still (Figure 3A). The still consisted of cotton wicks (Zorb®) placed through a large disc of ethylene-vinyl acetate (EVA) foam with the purpose of transporting water to the interface on top of the foam while remaining thermally insulated from the cold ocean water below. EVA provides good insulation while being highly durable and shock resistant. The entire surface of the still was covered with a polyvinyl chloride plastic dome to recondense the generated steam. PVC was chosen over other polymers as it allowed the most solar radiation to reach the TiC interface both when dry and wet resulting in the highest evaporation rates when tested in a lab setting (Figure S8 and S9). To maintain structural integrity, a stainless-steel umbrella frame was used. The solar intensity was tested at various points both inside and outside of the frame to rule out the possibility of shading of the evaporation surface (Figure S10), with no significant differences observed. After recondensing, the water will then be transported through another wick around the perimeter of the solar still, where it will reach an exit tube and collect in an independent collection bag. The freshwater collection wick is raised and shielded to avoid contamination from saltwater.

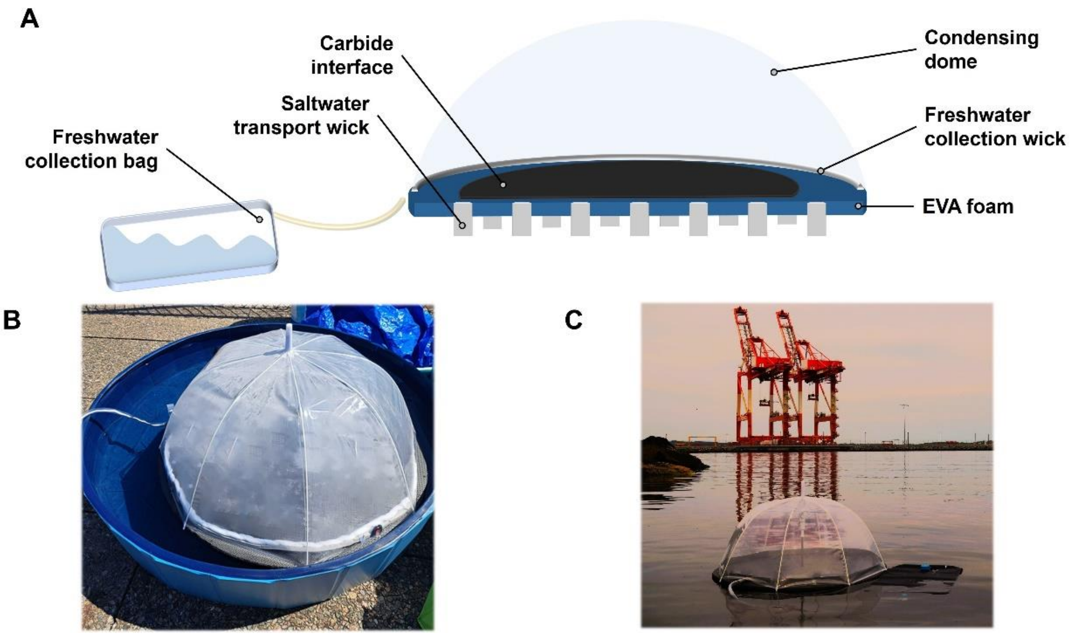

Figure 3: (A) Schematic of TiC floating solar still. (B) Rooftop testing location in pool filled with water taken from Halifax Harbour. (C) Testing directly in the Halifax Harbour (Atlantic Ocean water).

Initial outdoor testing was conducted on a rooftop inside of a pool containing water collected from the Halifax Harbour (latitude: 44° 36' 59.99" N, longitude: -63° 32' 59.99" W) as shown in Figure 3B and the evaporated water was collected into a glass container (Supplementary video 1). The solar still was tested for five consecutive days ranging from mostly cloudy to sunny, and the solar radiation was tracked over the course of each day (Figure 4A). The results of the rooftop testing are summarized in Figure 4B. First, the solar still was tested using a blank interface for comparison. This afforded a rate of 0.35 L m^{-2} day^{-1}, equating to a solar water generation efficiency of 4% using the following equation:

$$\eta_{still} = \frac{m_{H_2O}\Delta_{vap}H_m}{A_{still}\int q_{solar}(t)dt} \tag{1}$$

where η_{still} is the solar-to-water efficiency, m_{H_2O} is the mass of freshwater collected daily, A_{still} is the solar still evaporation area, and the bottom term gives the total daily solar flux on the surface of the solar still. When loaded with TiC NPs, the solar still generated more freshwater, affording rates of 2.03 L m^{-2} day^{-1} on a mostly cloudy day (3.67 kW m^{-2}) up to 3.67 L m^{-2} day-

[1] on a fully sunny day (6.56 kW m^{-2}). The maximum solar freshwater production efficiency was 40% and remains high on both sunny and cloudy days. It should be noted that the testing location (Halifax, Canada) has a more northernly latitude, with the peak sunlight intensity reaching an equivalent of about 0.84 suns, or 84%, compared to AM1.5. All testing conditions including daily sunlight intensities, ambient temperature, wind speed, and evaporation surface temperatures are summarized in Figure S11 and Table S1.

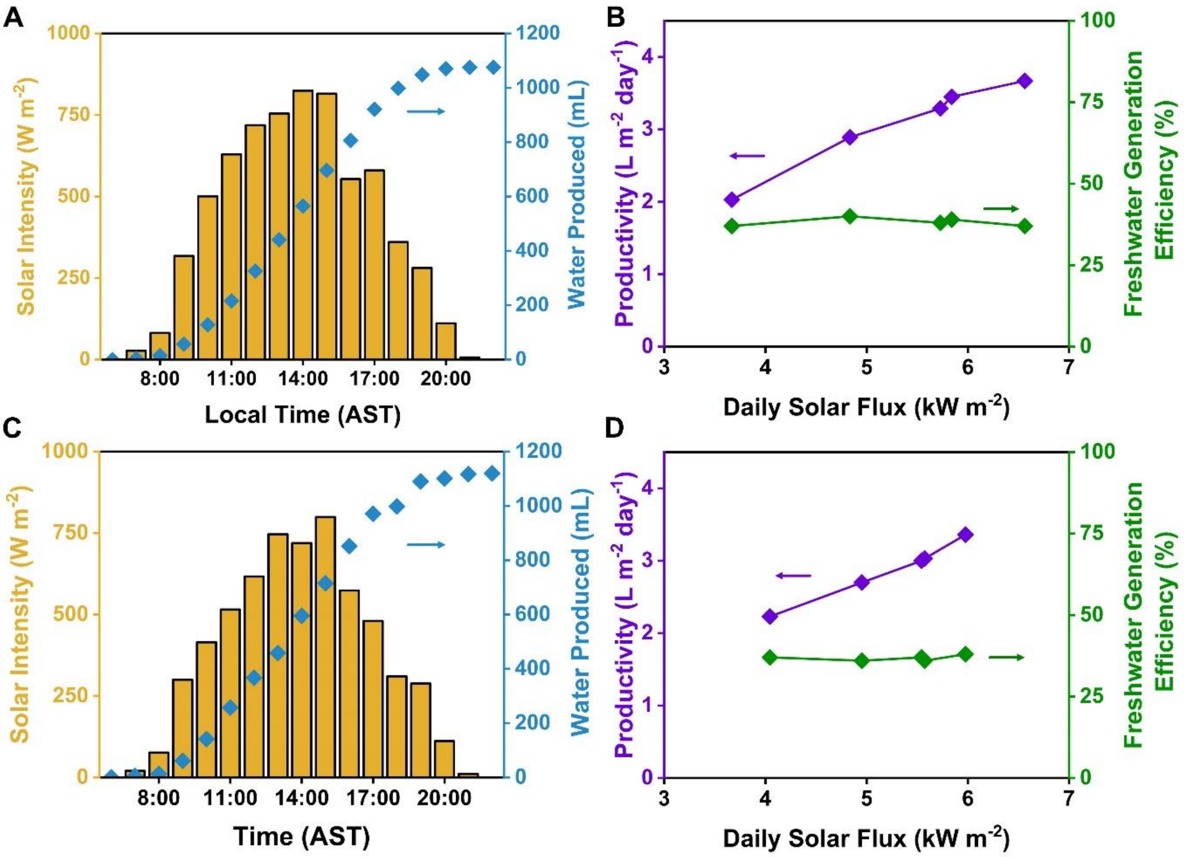

Figure 4: (A) Sample solar radiation and freshwater production chart for rooftop pool testing on a sunny day with afternoon intermittent cloud. (B) Freshwater generation rates (red, left) and efficiencies (green, right) for rooftop experiments. (C) Sample solar radiation and freshwater production chart for harbour testing on a sunny with afternoon intermittent cloud. (B) Freshwater generation rates (red, left) and efficiencies (green, right) for the harbour experiments.

After testing the performance of the solar still in the rooftop pool, it was deployed in the Atlantic Ocean (Halifax, Canada) over five full days (Figure 3C). The chosen location is nearby a large seaport and has had ongoing concern over elevated levels of toxic heavy metals. It is a heavily traversed route by both boats and ships and has additional tidal currents and moderate wave activity. This provided a challenging environment for the floating solar still to generate water as a real-world deployment test. Over the days of study, a range of sunny to cloudy days were encountered (Figure 4C and Table S2). As shown in Figure 4D, the max output was 3.36 L m^{-2} day^{-1} and the still produced at a rate of 2.23 L m^{-2} day^{-1} on a fully cloudy day. The solar-to-water generation efficiencies were once again similar regardless of the intensity of incoming light at 36-38%, just slightly below the rooftop experiments. This is likely due to an increased conduction of heat from the interface to the water below due to ocean currents, which could slightly decrease the overall efficiency.

After the five full days of testing, the solar still was deployed a final time to collect a purified water sample, and the microbial content was measured using cellular adenosine triphosphate (cATP) assay (Figure 5A). This gives a snapshot of the total biological concentration in each sample. The heat generated by the TiC NPs has the potential to destroy microbes and avoid fouling of the membrane and water transport system within the still. The cATP levels of water taken directly from the Halifax harbour testing site were compared to the desalinated sample. Another water sample was collected under controlled lab conditions with a freshly prepared TiC interface and collected using a closed quartz vessel that had been fully disinfected. The cATP concentration in both the solar still and laboratory evaporation samples were decreased significantly to 0.48 ± 0.17 and 0.25 ± 0.02 pg mL^{-1}, respectively, compared to the harbour water (123 ± 40 pg mL^{-1}). Both desalinated samples were below the guidelines set by Health Canada of 1 pg cATP mL^{-1} and are approaching the standard of high purity water which is set at 0.1 pg cATP mL^{-1}.[61] The cATP values for water samples from the solar still was only slightly higher than the water desalinated in the lab, which is most likely due to the rigorous cleaning process used for glassware before collecting the water. In contrast, the solar still had been used for rooftop studies and out on the harbour for two weeks without any cleaning before collecting the sample.

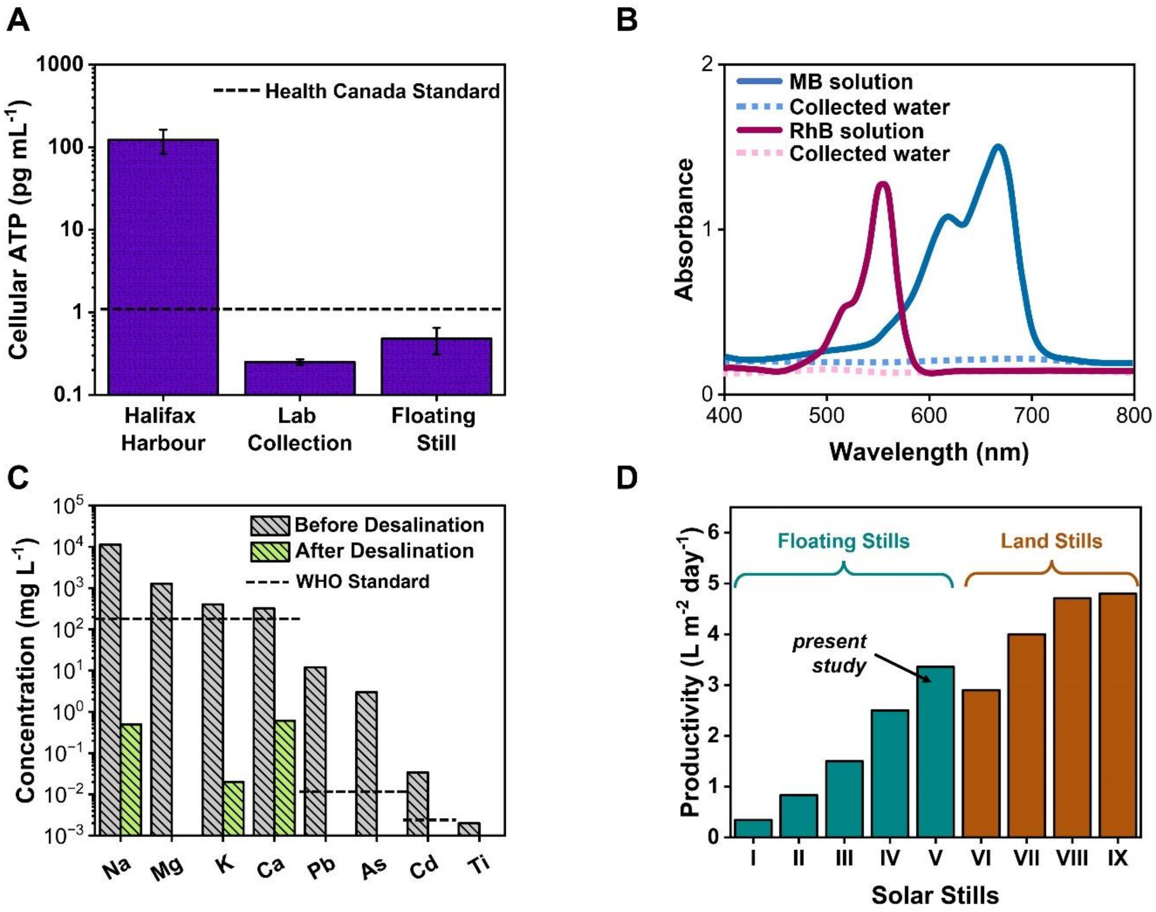

Figure 5: (A) ATP test results on logarithmic scale. (B) MB and RhB solutions before (solid lines) and after (dotted lines) solar evaporation. (C) ICPMS ion concentration results before (grey) and after (green) desalination. (D) Productivity of select solar stills in literature.

Following up on these results, dye separation and degradation experiments were conducted using both methylene blue (MB) and rhodamine B (RhB) under simulated 1 sun illumination in the lab (1000 W m^{-2}). First, solutions of each dye were prepared, and the absorbance spectra was compared to the collected water after evaporation (Figure 5B). The dye absorbance in the collected water was negligible, indicating no contamination from either dye. Secondly, the absorbance intensity of the dye in the source water was tested after various evaporation times. As seen in Figure S12, the concentration dropped by 60% for MB and 32% for RhB and this decrease in dye concentration was higher than when a blank evaporator was used. This indicates the potential for photothermally induced organic pollutant degradation using the TiC NPs and floating interfaces. The collected water was also tested for various ions using inductively coupled plasma mass spectrometry (ICPMS) to verify the extent of purification (Figure 5C). Results show that all tested ions from salt and heavy metal impurities are decreased by 3-5 orders of magnitude, putting the levels well below those set by the WHO.

The proposed solar still was compared to various passive floating solar stills, as well as several passive land stills (Figure 5D and Table S3). The TiC based device (current work) obtained higher daily productivity values than any floating solar still reported to date and is even higher than some of the more productive land-based solar stills reported. This can be attributed to the strong balance of water transport, interface thermal insulation, and high photothermal efficiency of the TiC NPs worked into the design. Furthermore, in previous studies it has been noted that when asymmetrically shaped condensation covers are used, if the solar still doesn't maintain a north to south orientation there would be a greater transmission loss through the side walls. The still was overturned during the ocean experiments causing damage and shortening the lifespan or requiring more frequent maintenance.[53] The symmetry of the still used in this work means that any orientation will have the same extent of transmission. Additionally, the large footprint of the still and slight flexibility of the EVA foam made it easily glide over incoming waves and avoid splashing over of water onto the surface.

Even though the efficiencies of land stills are slightly higher than any floating solar stills for desalination, they generally cost more to install and run.[62] This is in part because the ocean water must be continuously transported to the still and contained within basins. The additional use of land makes them potentially less desirable than floating solar stills. To further compare our proposed technology with other floating and land solar stills, we completed a basic cost analysis of the solar still built for this study. The method used was adapted from Fath *et al*. and Bait *et al*. to calculate the cost per litre (CPL) using the still.[63,64] This included the initial investment cost, along with estimated annual interest rates (10%), service life (2 years), and operation days per year (320 days). Additional values used throughout the calculations, including material cost, water purchase price, interest rate, etc., and are tabulated in Table S4.

The wholesale prices for TiC NP synthesis and solar still components were sourced from the Alibaba website. Electricity (0.11 \$ kwh^{-1}) and water prices (0.004 \$ L^{-1}) were taken from Nova Scotia Power and Halifax Municipal Water, respectively. Annual cost includes possible cleaning of still cover, replacement of wicks, and regular collection of distilled water. To account for seasonal solar intensity fluctuations, the average daily insolation for the year was used in the calculation.[65] This contrasts with most reports which use the production values in peak summer months for calculations. For this reason, there was assumed to be a linear trend between water production and sunlight intensity. We chose two different locations, the first was Halifax, Canada and the second was a more likely solar desalination destination of San Diego, California. The average daily insolation values were 11.8 and 19.6 kW m^{-2} for Halifax and San Diego, respectively and afforded CPL values of \$0.0086 and \$0.0052 L^{-1}. Comparing this to some of the most productive solar stills (Table S4), the proposed still has the lowest CPL and is comparable in productivity to some of the best performing land stills. The payback periods for the solar still were 290 days in Halifax, and 215 days in California. Interestingly, when assuming a productivity equal to the peak summer insolation as done in other reports, the CPL decreases to \$0.0045 L^{-1} in Halifax. The selling price of the distilled water in the calculations was the price from the local water utilities, though generally the cost of distilled water is assumed to be much higher (~\$0.15 L^{-1} vs \$0.03 L^{-1}) for water cost analyses.[53] This would further increase the economic efficiency of the proposed still.

2.3 Simultaneous Desalination and Electricity Generation

The generation of a relatively large temperature gradient between the evaporation interface of the solar still and the ocean water below can be used to generate electricity.[66] This process, known as thermoelectric generation, make use of the Seebeck effect where the flow of charge carriers at semiconductor p-n junctions induces an electrical current and voltage. Coupling this process with solar desalination has been proposed with some examples of laboratory scale studies and has been incorporated into a few of the land solar stills.[55–57,67] It has yet to be studied with a floating solar still but has the potential to power onboard devices such as small water quality monitors or fans to enhance evaporation. The thermoelectric generators (TGs) were added to the solar still by insetting them within the foam support. They were adhered to aluminum heat sinks which protrude below the still (Figure S13). The TGs were set in series and connected to a buck boost power converter to supply stabilized power to the load. As a proof of concept, a small fan and USB-C port for phone charging were explored (Figure 6A).

Testing was completed in a pool containing Halifax Harbour water directly beside the harbour in February, where the average air temperature during the testing period was 0 °C. The ocean temperature was also 0 °C, and the surface of the still during operation was 32 °C. Even though the ambient temperature was lower than when tested during the summer, temperature difference between the interface and the bulk water was very similar. At peak solar radiation (13:00), 98 mL of water was collected for the hour, displaying the utility of the solar still even at freezing temperatures (Figure 6B). The evaporation efficiency peaked at 33% on the testing day, compared to 38% during summertime testing. This can be attributed to the lower air and wind temperatures, which would increase the convective heat losses during the process. On testing day, the maximum induced open-circuit voltage ($V_{open\text{-}circuit}$) was measured to be 3.34 V, with the short-circuit current ($I_{short\text{-}circuit}$) reaching 486 mA (Figure 6C). This demonstrates the year-round utility of the solar still for simultaneous water and electricity generation. To estimate the maximum power output of the TG solar still, an external resistor (10 Ω) close to the internal resistance of the TG series (10.64 Ω) was connected. The circuit resistance was calculated using the method proposed by Tsang *et al.* (Thevenin equivalent resistance),[68] which afforded a maximum power output of 1.32 W (Figure 6D).

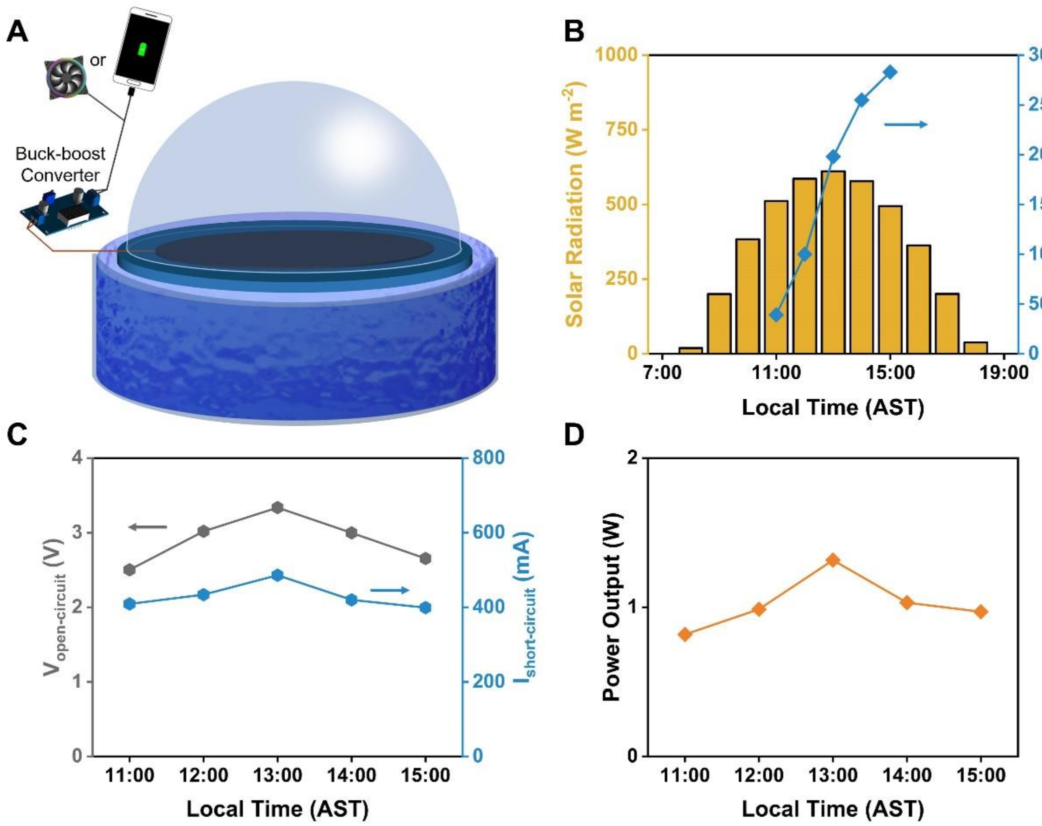

Figure 6: (A) Schematic of thermoelectric generation setup to power either a small fan or charge a smartphone. (B) Solar intensity, and water production on testing day (February 19th, 2024, from 11:00 until 15:00). (C) Open-circuit voltage (red) and short-circuit current (green) measured each hour of testing. (D) Maximum power output of the TG TiC solar still when connected to a 10 Ω resistor (equal to internal TG resistance).

After measuring the power output, the resistor was removed, and a fan was connected to the circuit. The fan can be operated without the buck-boost converter and was tested by connecting the terminals on the fan directly to the protruding wires of the TG solar still (Supplementary video 2). Reconnecting the buck-boost converter and connecting the circuit to a USB-C cord, the TG solar still can charge a cell phone, albeit at a slower rate compared to a home electrical outlet (Supplementary videos 3 & 4). This demonstrates the expanded utility of the solar still for powering small devices onboard such as sensors or for quality monitoring. The combination of desalination and thermoelectric generation has gained interest in the field, with many reports of lab-scale thermoelectric generation using simulated sunlight.[56,57,66–68] This however is the first example reported of a scaled up floating solar still to incorporate thermoelectric generation for real world utility**.**

3. Conclusions

The TiC NPs based solar still presented herein has been shown to generate freshwater from Atlantic Ocean at the highest productivity for a floating solar still reported to date. This marks a promising method of converting waste tire rubber into a value-added product for highly environmentally friendly solar desalination. The still design, matched with the high photothermal efficiency of the TiC coating, allows for such efficient desalination. The still can generate freshwater at a rate of 3.67 L m^{-2} day^{-1} corresponding to a solar efficiency of up to 40%. This efficiency remains over time when deployed in the ocean with waves, currents, wind, and sediment to deal with. The TMC still effectively resists microbe growth and decreases all tested ions by 3-5 orders of magnitude. In both cases the collected water is far below levels set by Health Canada and the WHO, both of which have some of the strictest guidelines worldwide. The still is also highly cost effective, producing water with a CPL as low as 0.5 ¢ L^{-1} over the lifetime of the still, with repayment in only 290 days in Halifax, Canada. This makes the still the most cost effective floating still to date and is very competitive with many top performing land stills. Finally, thermoelectrically harvesting the remaining waste heat, the still provides a peak power generation of 1.32 W, while maintaining a desalination efficiency of 33% in the middle of winter. The efficient heat generation of the TiC NPs benefits from the very cold ocean water below to reach such high electricity generation. The power generated is sufficient to run fans, and even charge a phone which highlights the potential utility for onboard electrics that might be needed.

4. Experimental

4.1 Materials

Titanium dioxide (TiO_2, 99.9%, 18 nm), was purchased from U.S. Research Nanomaterials. Magnesium powder (Mg, 99.8%, 325 mesh) was purchased from Alfa Aesar. Hydrochloric acid (HCl, ≥ 99%), nitric acid (HNO_3, ≥ 99%), methylene blue (>95%) and rhodamine B (>95%) were purchased from Sigma Aldrich. Deionized water (DI water, 18.2 MΩ cm) was obtained from Sartorius Arium water purification system. Polyester filter fabric (10 µm) was purchased from McMaster-Carr. Saltwater was obtained from the Atlantic Ocean (coordinates: 44°38'23.7" N 63°36'48.0" W). Zorb® Fabric was purchased from Wazoodle Fabrics. EVA foam (2.5 cm thick), stainless steel strapping (5 cm x 3mm), PVC transparent umbrella (0.8 m diameter), magnets, and Woods™ camp shower (5 L) were purchased from Canadian Tire. Solar intensity was measured using a TenMars TM-206 digital pyranometer. Wind speed, humidity, and outdoor ambient temperature were measured using a Kestrel 3000 pocket weather meter. All condition data was compared with data from Environment and Climate Change Canada for Halifax Shearwater (coordinates: 44°38'06.7" N 63°31'32.1" W). During evaporation experiments, temperatures within the still were monitored using either a Perfect Prime IR0005 or a K-type thermocouple. Akozon 40x40 mm semiconductor thermoelectric power generator modules (SP1848-27415) and the buck-boost power converter (Kananana 1.2-24 V step-up, step-down) were purchased from Amazon. The TEG generated voltage and current were measured using a digital multimeter (VSense U1233A).

4.2 Characterization Techniques

Powder X-ray diffraction (XRD) spectra were collected using a Proto AXRD® Benchtop with a Cu Kα radiation (λ = 1.54 Å). Powders were packed into a sample well of a resin holder. Absorbance and reflectance spectra were recorded on an Agilent CARY 5000 UV-Vis-NIR spectrometer. For liquid absorbance measurements, dispersions were placed into a quartz cuvette, and the spectrometer was background corrected using deionized water. For film samples, an external diffuse reflectance accessory with a 150 mm integrating sphere was used. The instrument was used in double beam mode using reduced slit height and was standard calibrated using a zero/baseline correction. Absorbance values were calculated from reflectance data using the following equation:

$$A = (1 - R)\ x\ 100\%$$

where A and R are absorbance and the measured reflectance, respectively. There is no transmission through the interfaces so it can be disregarded. Scanning electron microscopy (SEM) images were obtained on a Hitachi S-4700 electron microscope. Transmission electron microscopy (TEM) images were taken on a FEI TechaniTM 12 electron microscope with an accelerating voltage of 120 kV. TEM samples were prepared by drop-casting nanoparticle suspensions onto a 200-mesh carbon coated copper grid. The images were analyzed using ImageJ software. Inductively coupled plasma mass spectrometry (ICP-MS) measurements were performed on a Thermo Scientific X-Series 2 spectrometer and the standards were obtained from SCP Science.

4.3 Synthesis of Tire Char

Biochar synthesis was adapted from a previously reported anaerobic pyrolysis process.[58] Briefly, waste tire rubber was ground into a fine crumb, and subsequently pyrolyzed at 500 °C for 1 h under an Ar atmosphere. After cooling to ~100 °C, the reaction mixture was quenched in cold deionized water. The water was then heated to boiling for 10 minutes. The biochar was collected via filtration and the solid product was washed with water until the filtrate ran clear. The resulting biochar was dried and finely ground using a mortar and pestle, followed by sieving to ≤ 250 µm. The sieved biochar was then added to a beaker equipped with a magnetic stir-bar and reacted with concentrated HNO_3 for 30 minutes. Afterwards, the reaction was filtered, and the acid-treated biochar was rinsed with deionized water until the filtrate was neutral. The biochar was dried in an oven at 100 °C for 2 days.

4.4 Synthesis of TiC NPs

Titanium carbide NPs were prepared according to a previously reported procedure.[59] Briefly, in a nitrogen filled glovebox, 1.0 g of the corresponding metal oxide (TiO_2 ZrO_2, or HfO_2) was mixed with waste tire char (0.30 g) and magnesium (1.20 g) powders using a mortar and pestle until a homogenous mixture was obtained. The mixture was transferred to a stainless-steel combustion boat and placed into a quartz tube. After purging with argon gas for 15 min in a Lindberg Blue MTM furnace, the mixture was heated to 950 °C at a ramp rate of 10 °C min^{-1} and held for 4 hours. The reaction mixture was cooled to ambient temperature and transferred to a glass beaker. 6.0 M HCl (20 mL) was added to the reaction product and was sonicated for 1 hour. Carbides were washed in distilled water (3 x 10 mL) by sonication, centrifugation, and pouring off the supernatant each time. After the third wash, the NPs were filtered and rinsed with acetone, followed by ethanol, then dried in an oven.

4.5 Preparation of TiC NP Evaporation Interface

The TiC evaporation interface was prepared by spray-coating under vacuum using a setup built in house (Figure S6). A given volume of 0.1 g mL^{-1} solution of TiC NPs was sprayed onto a 65 cm diameter polyester filter (McMaster-Carr, 10 μm) to give a particle loading of 1.0 g m^{-2}. The interface was then allowed to air dry to increase adsorption of the NPs to the filter. The total evaporation area for use with the solar still is 0.33 m^2.

4.6 Preparation of Solar Still

EVA foam (2.5 cm thick) was cut into an 80 cm diameter disc, and 3 mm holes (i.e. 68 in total) were drilled through the foam to cover 2.5% of the total surface area. Absorbent cotton (Zorb®) was rolled into 3 mm wicks and inserted into each hole. An additional ring of EVA foam (2.5 x 2.5 cm, 78.5 cm inner diameter) was cut and adhered to the foam base to elevate a freshwater wick that circled the outer part of the foam support (main article, Figure 2). To further avoid splashing of water onto the collection wick, stainless steel strapping (5 cm x 3mm) was inserted upright into the foam around the circumference of the solar still (Figure S14). A 6 mm hole was drilled through the center of the foam support to insert the condensation dome, which was further secured by adding magnetic snaps around the outside of the frame. The net weight of the solar still is 1.5 kg.

4.7 Rooftop Desalination Experiment

The TiC solar still was floated in a 1.5 m diameter pool that was filled with water taken from the Halifax Harbour (latitude: 44° 36' 59.99" N, longitude: -63° 32' 59.99" W). Tested started at 7:00 each testing day and ran until 21:00, with water being continuously collected. Water was collected through the outlet tube into a glass container and the amount collected was measured hourly. Solar intensity, ambient and solar still surface temperature, and wind speed were also recorded hourly.

4.8 Harbour Desalination Experiment

The TiC solar still was floated directly in the Halifax Harbour (latitude: 44° 36' 59.99" N, longitude: -63° 32' 59.99" W), starting at 7:00 and ending at 21:00. Water was continuously collected through the outlet tube into a modified Woods™ brand camping shower, designed to be watertight. The amount of water collected was measured at the end of the day. The solar still was tied off to a post to prevent it from drifting. Solar intensity, ambient and solar still surface temperature, and wind speed were also recorded hourly.

4.9 ATP Assay Measurements

ATP measurements were taken using the LUMINULTRA ATP test kit QuenchGone™ Aqueous (QGA). For analysis, the samples were collected in sterile 50 mL Falcon tubes and inverted prior to analysis to ensure complete cellular dispersion. Samples were passed over a 0.45 µm syringe filter to retain all biomass in the filter. An elution reagent was poured into the filter to breakdown cells and liberate ATP. The filtrate was collected into a dilution tube and was then mixed with the luminase enzyme. The prepared sample was placed into a luminometer to obtain the relative light units (RLU) of cellular ATP. The RLU is proportional to the amount of biomass present in the sample. For the lab scale desalination only 2 replicates were performed, while for the harbour water and solar still analysis was done 3 times. Scanning electron microscopy (SEM) images were obtained on a Hitachi S-4700 electron microscope. Inductively coupled plasma mass spectrometry (ICP-MS) measurements were performed on a Thermo Scientific X-Series 2 spectrometer and the standards were obtained from SCP Science.

4.10 Dye Studies

For dye studies, 3.0 mM stock solutions were made by adding 0.3 mmol of either methylene blue (MB) or rhodamine B (RhB) to 100 mL of deionized H_2O. TiC evaporation interfaces were floated on the stock solutions inside a closed quartz vessel with a sloped cover to recondense water vapor. Water samples were taken from the collection side of the vessel and the absorbance was tested by UV Vis. To monitor the concentration of the stock solution during evaporation, aliquots were taken at the designated times (5, 10, 15, 30, 60, and 120 minutes). After UV Vis analysis, the sample was added back to the vessel and deionized water was added to maintain the overall water level. Blank experiments were run to determine how much of the dyes were being taken up by the evaporation interface.

Acknowledgements

The authors thank funding from the Natural Sciences and Engineering Research Council of Canada (NSERC) Discovery and Alliance Grants, Canada Foundation for Innovation, Research Nova Scotia, Killam Trusts, and Ocean Frontier Institute. KN and MA thank NSERC and Joy M. Cunningham endowment, respectively for research awards and MM for graduate fellowship from the Sumner Foundation. T. Hynes and the Clean Technologies Research Institute are thanked for access and assistance with SEM analysis. Dr. S. A. Martell and the Electron Microscope Core Facility are thanked for assistance with TEM analysis. Prof. H. Andreas is thanked for access to the UV-Vis-NIR absorbance spectrometer.

Conflict of Interests

The authors declare no conflict of interests.

Supporting Information

Supporting Information is available. It contains additional characterization data (XRD, SEM, TEM, UV Vis) for the tire rubber char, TiC NPs, and evaporation interfaces. It also contains all solar still design concepts and studies, as well as rooftop pool and harbor experiments including environmental conditions. All values used for the economic analysis calculations are included as well.

References

1. Kummu M, Guillaume JHA, de Moel H, et al. The world's road to water scarcity: shortage and stress in the 20th century and pathways towards sustainability. *Sci Rep*. 2016;6(1):38495.
2. Veldkamp TIE, Wada Y, Aerts JCJH, et al. Water scarcity hotspots travel downstream due to human interventions in the 20th and 21st century. *Nat Commun*. 2017;8(1):15697.
3. Elimelech M, Phillip WA. The Future of Seawater Desalination: Energy, Technology, and the Environment. *Science (1979)*. 2011;333(6043):712-717.
4. Sharaf MA, Nafey AS, García-Rodríguez L. Thermo-economic analysis of solar thermal power cycles assisted MED-VC (multi effect distillation-vapor compression) desalination processes. *Energy*. 2011;36(5):2753-2764.
5. Zhao D, Xue J, Li S, Sun H, Zhang Q dong. Theoretical analyses of thermal and economical aspects of multi-effect distillation desalination dealing with high-salinity wastewater. *Desalination*. 2011;273(2):292-298.

6. Greenlee LF, Lawler DF, Freeman BD, Marrot B, Moulin P. Reverse osmosis desalination: Water sources, technology, and today's challenges. *Water Res*. 2009;43(9):2317-2348.
7. Peñate B, García-Rodríguez L. Current trends and future prospects in the design of seawater reverse osmosis desalination technology. *Desalination*. 2012;284:1-8.
8. Qasim M, Badrelzaman M, Darwish NN, Darwish NA, Hilal N. Reverse osmosis desalination: A state-of-the-art review. *Desalination*. 2019;459:59-104.
9. AlSawaftah N, Abuwatfa W, Darwish N, Husseini G. A Comprehensive Review on Membrane Fouling: Mathematical Modelling, Prediction, Diagnosis, and Mitigation. *Water*. 2021;13(9).
10. Dhakal N, Salinas-Rodriguez SG, Hamdani J, et al. Is Desalination a Solution to Freshwater Scarcity in Developing Countries? *Membranes*. 2022;12(4).
11. Ghaffour N, Bundschuh J, Mahmoudi H, Goosen MFA. Renewable energy-driven desalination technologies: A comprehensive review on challenges and potential applications of integrated systems. *Desalination*. 2015;356:94-114.
12. Min X, Zhu B, Li B, Li J, Zhu J. Interfacial Solar Vapor Generation: Materials and Structural Design. *Acc Mater Res*. 2021;2(4):198-209.
13. Zhou L, Li X, Ni GW, Zhu S, Zhu J. The revival of thermal utilization from the Sun: interfacial solar vapor generation. *Natl Sci Rev*. 2019;6(3):562-578.
14. Luo X, Shi J, Zhao C, Luo Z, Gu X, Bao H. The energy efficiency of interfacial solar desalination. *Appl Energy*. 2021;302:117581.
15. Yu S, Gu Y, Chao X, Huang G, Shou D. Recent advances in interfacial solar vapor generation: clean water production and beyond. *J Mater Chem A Mater*. 2023;11(12):5978-6015.
16. Gu X, Fan C, Sun Y. Multilevel design strategies of high-performance interfacial solar vapor generation: A state of the art review. *Chemical Engineering Journal*. 2023;460:141716.
17. Luo X, Shi J, Zhao C, Luo Z, Gu X, Bao H. The energy efficiency of interfacial solar desalination. *Appl Energy*. 2021;302:117581.
18. Ashish CK, Sujith Kumar CS, Raj AK, Ubaidulla CT, Inbaoli A, Jayaraj S. Experimental evaluation on the capillarity effect of different wicking structure incorporated in a patterned absorber facilitating solar interfacial evaporation. *J Therm Anal Calorim*. 2022;147(17):9865-9886.
19. Yang T, Lin H, Lin KT, Jia B. Carbon-based absorbers for solar evaporation: Steam generation and beyond. *Sustainable Materials and Technologies*. 2020;25:e00182.
20. Dao VD, Choi HS. Carbon-Based Sunlight Absorbers in Solar-Driven Steam Generation Devices. *Global Challenges*. 2018;2(2):1700094.
21. Xie Z, Wang H, Geng Y, et al. Carbon-Based Photothermal Superhydrophobic Materials with Hierarchical Structure Enhances the Anti-Icing and Photothermal Deicing Properties. *ACS Appl Mater Interfaces*. 2021;13(40):48308-48321.
22. Xiao L, Chen X, Yang X, Sun J, Geng J. Recent Advances in Polymer-Based Photothermal Materials for Biological Applications. *ACS Appl Polym Mater*. 2020;2(10):4273-4288.

23. Wang M, Huang X, Yang H. Photothermal-Responsive Crosslinked Liquid Crystal Polymers. *Macromol Mater Eng*. 2023;n/a(n/a):2300061.
24. Ibrahim I, Seo DH, McDonagh AM, Shon HK, Tijing L. Semiconductor photothermal materials enabling efficient solar steam generation toward desalination and wastewater treatment. *Desalination*. 2021;500:114853.
25. Tan KW, Yap CM, Zheng Z, Haw CY, Khiew PS, Chiu WS. State-of-the-Art Advances, Development, and Challenges of Metal Oxide Semiconductor Nanomaterials for Photothermal Solar Steam Generation. *Adv Sustain Syst*. 2022;6(4):2100416.
26. Dasog M. Transition Metal Nitrides Are Heating Up the Field of Plasmonics. *Chemistry of Materials*. 2022;34(10):4249-4258.
27. Farid MU, Kharraz JA, Wang P, An AK. High-efficiency solar-driven water desalination using a thermally isolated plasmonic membrane. *J Clean Prod*. 2020;271:122684.
28. Fuzil NS, Othman NH, Alias NH, et al. A review on photothermal material and its usage in the development of photothermal membrane for sustainable clean water production. *Desalination*. 2021;517:115259.
29. Razaqpur AG, Wang Y, Liao X, Liao Y, Wang R. Progress of photothermal membrane distillation for decentralized desalination: A review. *Water Res*. 2021;201:117299.
30. Lee YM, Kim SE, Park JE. Strong coupling in plasmonic metal nanoparticles. *Nano Converg*. 2023;10(1):34.
31. Margeson MJ, Dasog M. Plasmonic metal nitrides for solar-driven water evaporation. *Environ Sci (Camb)*. 2020;6(12):3169-3177.
32. Margeson MJ, Atwood M, Monfared YE, Dasog M. Plasmonic group 4 transition metal carbide interfaces for solar-driven desalination. *Aggregate*. 2024;n/a(n/a):e531.
33. Ai S, Ma M, Chen YZ, Gao XH, Liu G. Metal-ceramic Carbide Integrated Solar-driven Evaporation Device Based on ZrC Nanoparticles for Water Evaporation and Desalination. *Chemical Engineering Journal*. 2022;429:132014.
34. Ihsanullah I. Potential of MXenes in Water Desalination: Current Status and Perspectives. *Nanomicro Lett*. 2020;12(1):72.
35. Hu X, Zhu J. Tailoring Aerogels and Related 3D Macroporous Monoliths for Interfacial Solar Vapor Generation. *Adv Funct Mater*. 2020;30(3):1907234.
36. Xu Z, Ran X, Wang D, Zhong M, Zhang Z. High efficient 3D solar interfacial evaporator: Achieved by the synergy of simple material and structure. *Desalination*. 2022;525:115495.
37. Chang C, Liu M, Pei L, Chen G, Wang Z, Ji Y. Porous TiNO Solar-driven Interfacial Evaporator for High-efficiency Seawater Desalination. *AIP Adv*. 2021;11(4):045228.
38. Finnerty CTK, Menon AK, Conway KM, et al. Interfacial Solar Evaporation by a 3D Graphene Oxide Stalk for Highly Concentrated Brine Treatment. *Environ Sci Technol*. 2021;55(22):15435-15445.
39. Zang L, Finnerty C, Zheng S, et al. Interfacial solar vapor generation for desalination and brine treatment: Evaluating current strategies of solving scaling. *Water Res*. 2021;198:117135.
40. Sun Z, Zhang L, Liu L, et al. Optimal design for floating solar still by structural modification: A review. *Desalination*. 2023;566:116937.

41. Naghdi B, Heshmati FZ, Mahjoub F, et al. Salt precipitation challenge in floating interfacial solar water desalination systems. *Desalination*. 2023;565:116868.
42. Lv F, Miao J, Hu J, Orejon D. 3D Solar Evaporation Enhancement by Superhydrophilic Copper Foam Inverted Cone and Graphene Oxide Functionalization Synergistic Cooperation. *Small*. 2023;19(30):2208137.
43. Wang Z, Liu H, Chen F, Zhang Q. A three-dimensional printed biomimetic hierarchical graphene architecture for high-efficiency solar steam-generation. *J Mater Chem A Mater*. 2020;8(37):19387-19395.
44. Zhu F, Wang L, Demir B, et al. Accelerating solar desalination in brine through ion activated hierarchically porous polyion complex hydrogels. *Mater Horiz*. 2020;7(12):3187-3195.
45. Xu R, Wei N, Li Z, et al. Construction of hierarchical 2D/2D Ti3C2/MoS2 nanocomposites for high-efficiency solar steam generation. *J Colloid Interface Sci*. 2021;584:125-133.
46. Wang Y, Nie J, He Z, Zhi Y, Ma X, Zhong P. Ti3C2Tx MXene Nanoflakes Embedded with Copper Indium Selenide Nanoparticles for Desalination and Water Purification through High-Efficiency Solar-Driven Membrane Evaporation. *ACS Appl Mater Interfaces*. 2022;14(4):5876-5886.
47. Xu J, Wang Z, Chang C, et al. Solar-driven interfacial desalination for simultaneous freshwater and salt generation. *Desalination*. 2020;484:114423.
48. Liu Y, Tian J, Xu L, Wang Y, Fei X, Li Y. Multilayer graphite nano-sheet composite hydrogel for solar desalination systems with floatability and recyclability. *New J Chem*. 2020;44(46):20181-20191.
49. Du C, Huang C. A floating vapor condensation structure in a heat-localized solar evaporation system for facile solar desalination. *Appl Therm Eng*. 2022;201:117834.
50. Raihananda FA, Philander E, Lauvandy AF, et al. Low-cost floating solar still for developing countries: Prototyping and heat-mass transfer analysis. *Results in Engineering*. 2021;12:100300.
51. Liu Z, Song H, Ji D, et al. Extremely Cost-Effective and Efficient Solar Vapor Generation under Nonconcentrated Illumination Using Thermally Isolated Black Paper. *Global Challenges*. 2017;1(2):1600003.
52. Ni G, Zandavi SH, Javid SM, Boriskina S V, Cooper TA, Chen G. A salt-rejecting floating solar still for low-cost desalination. *Energy Environ Sci*. 2018;11(6):1510-1519.
53. Chen S, Zhao P, Xie G, et al. A floating solar still inspired by continuous root water intake. *Desalination*. 2021;512:115133.
54. Mohsenzadeh M, Aye L, Christopher P. Development and experimental analysis of an innovative self-cleaning low vacuum hemispherical floating solar still for low-cost desalination. *Energy Convers Manag*. 2022;251:114902.
55. Sun Y, Zhao Z, Zhao G, et al. Solar-driven simultaneous desalination and power generation enabled by graphene oxide nanoribbon papers. *J Mater Chem A Mater*. 2022;10(16):9184-9194.
56. Shoeibi S, Saemian M, Parsa SM, Khiadani M, Mirjalily SAA, Kargarsharifabad H. A novel solar desalination system equipped with thermoelectric generator, reflectors and

low-cost sensible energy-storage for co-production of power and drinking water. *Desalination*. 2023;567:116955.

57. Ren J, Chen L, Gong J, Qu J, Niu R. Hofmeister effect mediated hydrogel evaporator for simultaneous solar evaporation and thermoelectric power generation. *Chemical Engineering Journal*. 2023;458:141511.
58. Humagain G, MacDougal K, MacInnis J, et al. Highly efficient, biochar-derived molybdenum carbide hydrogen evolution electrocatalyst. *Adv Energy Mater*. 2018;8(29):1801461.
59. Margeson MJ, Monfared YE, Dasog M. Synthesis and Photothermal Properties of UV-Plasmonic Group IV Transition Metal Carbide Nanoparticles. *ACS Applied Optical Materials*. 2023;1(5):1004-1011.
60. Han W, Han D, Chen H. Pyrolysis of Waste Tires: A Review. *Polymers (Basel)*. 2023;15(7).
61. Liu J, He H, Xiao D, et al. Recent Advances of Plasmonic Nanoparticles and their Applications. *Materials*. 2018;11(10):1833.
62. Sanserwal M, Kumar Singh A, Singh P. Impact of materials and economic analysis of single slope single basin passive solar still: A review. *Mater Today Proc*. 2020;21:1643-1652.
63. Fath HES, El-Samanoudy M, Fahmy K, Hassabou A. Thermal-economic analysis and comparison between pyramid-shaped and single-slope solar still configurations. *Desalination*. 2003;159(1):69-79.
64. Bait O. Exergy, environ–economic and economic analyses of a tubular solar water heater assisted solar still. *J Clean Prod*. 2019;212:630-646.
65. Duan H, Wang T, Su Z, Pang H, Chen C. Recent progress and challenges in plasmonic nanomaterials. *Materials*. 2022;11(1):846-873.
66. Jaziri N, Boughamoura A, Müller J, Mezghani B, Tounsi F, Ismail M. A comprehensive review of Thermoelectric Generators: Technologies and common applications. *Energy Reports*. 2020;6:264-287.
67. Shoeibi S, Saemian M, Parsa SM, Khiadani M, Mirjalily SAA, Kargarsharifabad H. A novel solar desalination system equipped with thermoelectric generator, reflectors and low-cost sensible energy-storage for co-production of power and drinking water. *Desalination*. 2023;567:116955.
68. Saleque AM, Thakur AK, Saidur R, et al. rGO coated cotton fabric and thermoelectric module arrays for efficient solar desalination and electricity generation. *J Mater Chem A Mater*. 2024;12(1):405-418.